Biomedical Optics EXPRESS

Detection of cervical cancer based on photoacoustic imaging—the in-vitro results

Kuan Peng,[1] Ling He,[2] Bo Wang,[1,3] and Jiaying Xiao[1,*]

[1] *Department of Biomedical Engineering, School of Geosciences and Info-Physics, Central South University, Changsha, Hunan 410083, China*

[2] *Obstetrics & Gynecology Department, Second Xiangya Hospital, Central South University, Changsha, Hunan 410011, China*

[3] *College of Biology, Hunan University, Changsha, Hunan 410082, China*

[*] *xjycsu@gmail.com*

Abstract: In current clinical practice, the diagnosis of cervical cancer (CC) is mainly through the cervical screening followed by a necessary biopsy, but this method is labor consuming and expensive, and can only detect superficial lesions around the external cervical orifice. In contrast, photoacoustic imaging (PAI) is sensitive to the abnormal angiogenesis deep in the biological tissue, and may be capable for the intact scanning both around the external orifice and in cervical canal. In this paper, we for the first time put forward the photoacoustic diagnosis of CC. A total of 30 in-vitro experiments were carried out in this study, and the obtained depth maximum amplitude projection (DMAP) images were analyzed to evaluate the extent of the angiogenesis for different clinical stages of CC. Stronger absorption from the cervical lesions is observed relative to that of normal tissue. Paired t-test indicates that the difference in mean optical absorption (MOA) between normal tissue and cervical lesion has statistical significance with a confidential coefficient of 0.05. Statistical results also show that the MOAs of the cervical lesions are closely related to the severity of CC. These results imply that PAI may have great utility in the clinical diagnosis of CC.

OCIS codes: (170.5120) Photoacoustic imaging; (170.3880) Medical and biological imaging; (170.2150) Endoscopic imaging.

References and links

1. J. Ferlay, H. R. Shin, F. Bray, D. Forman, C. Mathers, and D. M. Parkin, "Estimates of worldwide burden of cancer in 2008: GLOBOCAN 2008," Int. J. Cancer **127**(12), 2893–2917 (2010).
2. D. M. Parkin, F. Bray, J. Ferlay, and P. Pisani, "Global cancer statistics, 2002," CA Cancer J. Clin. **55**(2), 74–108 (2005).
3. J. M. Agosti and S. J. Goldie, "Introducing HPV vaccine in developing countries--key challenges and issues," N. Engl. J. Med. **356**(19), 1908–1910 (2007).
4. I. M. Orfanoudaki, D. Kappou, and S. Sifakis, "Recent advances in optical imaging for cervical cancer detection," Arch. Gynecol. Obstet. **284**(5), 1197–1208 (2011).
5. D. Ferris, T. Cox, D. Connor, and V. Wright, *Modern Colposcopy Textbook and Atlas* (Lippincott Williams & Wilkins, 2011).
6. N. Thekkek, R. Richards-Kortum, "Optical imaging for cervical cancer detection: solutions for a continuing global problem," Nat. Rev. Cancer **8**(9), 725–731 (2008).
7. S. Triratanachat, S. Niruthisard, P. Trivijitsilp, D. Tresukosol, and N. Jarurak, "Angiogenesis in cervical intraepithelial neoplasia and early-staged uterine cervical squamous cell carcinoma: clinical significance," Int. J. Gynecol. Cancer **16**(2), 575–580 (2006).
8. R. A. Drezek, T. Collier, C. K. Brookner, A. Malpica, R. Lotan, R. R. Richards-Kortum, and M. Follen, "Laser scanning confocal microscopy of cervical tissue before and after application of acetic acid," Am. J. Obstet. Gynecol. **182**(5), 1135–1139 (2000).
9. T. Collier, M. Follen, A. Malpica, and R. Richards-Kortum, "Sources of scattering in cervical tissue: determination of the scattering coefficient by confocal microscopy," Appl. Opt. **44**(11), 2072–2081 (2005).
10. D. Arifler, C. MacAulay, M. R. Follen, and R. Richards-Kortum, "Spatially resolved reflectance spectroscopy for diagnosis of cervical precancer: Monte Carlo modeling and comparison to clinical measurements," J. Biomed. Opt. **11**(6), 064027 (2006).

#221095 - $15.00 USD Received 27 Aug 2014; revised 20 Oct 2014; accepted 13 Nov 2014; published 15 Dec 2014

11. R. Drezek, C. Brookner, I. Pavlova, I. Boiko, A. Malpica, R. Lotan, M. Follen, and R. Richards-Kortum, "Autofluorescence microscopy of fresh cervical-tissue sections reveals alterations in tissue biochemistry with dysplasia," Photochem. Photobiol. **73**(6), 636–641 (2001).
12. L. Denny, L. Kuhn, A. Pollack, and T. C. Wright, Jr., "Direct visual inspection for cervical cancer screening: an analysis of factors influencing test performance," Cancer **94**(6), 1699–1707 (2002).
13. I. M. Orfanoudaki, G. C. Themelis, S. K. Sifakis, D. H. Fragouli, J. G. Panayiotides, E. M. Vazgiouraki, and E. E. Koumantakis, "A clinical study of optical biopsy of the uterine cervix using a multispectral imaging system," Gynecol. Oncol. **96**(1), 119–131 (2005).
14. W. Steller, J. Einenkel, L. C. Horn, U. D. Braumann, H. Binder, R. Salzer, and C. Krafft, "Delimitation of squamous cell cervical carcinoma using infrared microspectroscopic imaging," Anal. Bioanal. Chem. **384**(1), 145–154 (2006).
15. C. MacAulay, P. Lane, and R. Richards-Kortum, "In vivo pathology: microendoscopy as a new endoscopic imaging modality," Gastrointest. Endosc. Clin. N. Am. **14**(3), 595–620 (2004).
16. J. Gallwas, L. Turk, K. Friese, and C. Dannecker, "Optical coherence tomography as a non-invasive imaging technique for preinvasive and invasive neoplasia of the uterine cervix," Ultrasound Obstet. Gynecol. **36**(5), 624–629 (2010).
17. J. P. Culver, V. Ntziachristos, M. J. Holboke, and A. G. Yodh, "Optimization of optode arrangements for diffuse optical tomography: A singular-value analysis," Opt. Lett. **26**(10), 701–703 (2001).
18. H. Weingandt, H. Stepp, R. Baumgartner, J. Diebold, W. Xiang, and P. Hillemanns, "Autofluorescence spectroscopy for the diagnosis of cervical intraepithelial neoplasia," BJOG **109**(8), 947–951 (2002).
19. C. Murali Krishna, N. B. Prathima, R. Malini, B. M. Vadhiraja, R. A. Bhatt, D. J. Fernandes, P. Kushtagi, M. S. Vidyasagar, and V. B. Kartha, "Raman spectroscopy studies for diagnosis of cancers in human Uterine cervix," Vib. Spectrosc. **41**(1), 136–141 (2006).
20. D. Gius, M. C. Funk, E. Y. Chuang, S. Feng, P. C. Huettner, L. Nguyen, C. M. Bradbury, M. Mishra, S. Gao, B. M. Buttin, D. E. Cohn, M. A. Powell, N. S. Horowitz, B. P. Whitcomb, and J. S. Rader, "Profiling microdissected epithelium and stroma to model genomic signatures for cervical carcinogenesis accommodating for covariates," Cancer Res. **67**(15), 7113–7123 (2007).
21. D. Kerrigan, "Identifying Molecular Culprits of Cervical Cancer Progression," http://home.ccr.cancer.gov/inthejournals/archives/Gius_03.asp.
22. L. V. Wang and S. Hu, "Photoacoustic tomography: in vivo Imaging from organelles to organs," Science **335**(6075), 1458–1462 (2012).
23. L. Xi, S. R. Grobmyer, G. Zhou, W. Qian, L. Yang, and H. Jiang, "Molecular photoacoustic tomography of breast cancer using receptor targeted magnetic iron oxide nanoparticles as contrast agents," J. Biophotonics **7**(6), 401–409 (2014).
24. S. Manohar, S. E. Vaartjes, J. C. van Hespen, J. M. Klaase, F. M. van den Engh, W. Steenbergen, and T. G. van Leeuwen, "Initial results of in vivo non-invasive cancer imaging in the human breast using near-infrared photoacoustics," Opt. Express **15**(19), 12277–12285 (2007).
25. G. Ku, X. Wang, X. Xie, G. Stoica, and L. V. Wang, "Imaging of tumor angiogenesis in rat brains in vivo by photoacoustic tomography," Appl. Opt. **44**(5), 770–775 (2005).
26. R. Cubeddu, A. Pifferi, P. Taroni, A. Torricelli, and G. Valentini, "A solid tissue phantom for photon migration studies," Phys. Med. Biol. **42**(10), 1971–1979 (1997).
27. V. T. Chang, P. S. Cartwright, S. M. Bean, G. M. Palmer, R. C. Bentley, and N. Ramanujam, "Quantitative Physiology of the Precancerous Cervix In Vivo through Optical Spectroscopy," Neoplasia **11**(4), 325–332 (2009).
28. C. Kim, K. H. Song, F. Gao, and L. V. Wang, "Sentinel lymph nodes and lymphatic vessels: noninvasive dual-modality in vivo mapping by using indocyanine green in rats--volumetric spectroscopic photoacoustic imaging and planar fluorescence imaging," Radiology **255**(2), 442–450 (2010).
29. A. R. John, *Athematical Statistics and Data Analysis* (Cengage Learning, 2006).
30. J. L. Myers and A. D. Well, Research design and statistical analysis (Routledge, 2003).
31. J. Wei, "Pathology of Cervical Carcinoma," http://www.glowm.com/section_view/heading/Pathology%20of%20Cervical%20Carcinoma/item/230.
32. J. W. Sellors and R. Sankaranarayanan, "Colposcopy and Treatment of Cervical Intraepithelial Neoplasia: A Beginner's Manual," http://screening.iarc.fr/colpochap.php?chap=2.
33. B. Wang, J. L. Su, A. B. Karpiouk, K. V. Sokolov, R. W. Smalling, and S. Y. Emelianov, "Intravascular photoacoustic imaging," IEEE. J. Sel. Top. Quantum Electron. **16**(3), 588–599 (2010).
34. J. M. Yang, R. M. Chen, C. Favazza, J. Yao, C. Li, Z. Hu, Q. Zhou, K. K. Shung, and L. V. Wang, "A 2.5-mm diameter probe for photoacoustic and ultrasonic endoscopy," Opt. Express **20**(21), 23944–23953 (2012).
35. Z. Yuan and H. Jiang, "A calibration-free, one-step method for quantitative photoacoustic tomography," Med. Phys. **39**(11), 6895–6899 (2012).

1. Introduction

Cervical cancer (CC) is one of the most common malignancies in women worldwide [1], which is developed from the cervical intraepithelial neoplasia (CIN). CIN is majorly caused by the chronic infection of the cervix with the sexually transmitted human papillomavirus (HPV) [2]. Although vaccines against high risk HPV types have been developed recently, they cannot cover all oncogenic HPV subtypes, nor can they provide protection for older

#221095 - $15.00 USD Received 27 Aug 2014; revised 20 Oct 2014; accepted 13 Nov 2014; published 15 Dec 2014

women [3]. It has been proved that the treatment of CC critically depends on how early the cancer is detected. Currently, the diagnosis of CC is typically by cervical screening such as the Papanicolau or "Pap" smears to detect potentially precancerous changes, and an abnormal screening result may lead to colposcopical examination and recommend biopsy. Medical imaging is then involved to determine whether or not the cancer has spread if needed. Despite the fact that cervical screening has remarkably reduced the occurrence of CC, the confirming of the detected suspiciousness relies on the time/labor consuming and expensive biopsy, which can only give results at some selective spots. Thus some lesions may still be missing, or patients may be referred to unnecessary biopsies [4]. Furthermore, this method is only effective when detecting the superficial lesions around the external cervical orifice, while considerable number of the CC cases involved lesions in the cervical canal [5]. Therefore, there is still a need to develop new diagnosis technologies with high accuracy, deep penetration, larger scanning regions, and low cost for the routing tests of CC.

The development of cervical lesions leads to broad range of alterations in tissue optical properties [6]. Vascular changes in the cervical tissue can be found due to the abnormal generation of new blood vessels [7]. Because of the characteristic in the absorption spectrum of hemoglobin, optical absorption around the wavelengths of 420 nm, 542 nm and 577 nm is increased remarkably. The application of acetic acid elevates the mean scattering coefficient of precancerous tissue approximately three times that of normal epithelium, making abnormal tissue appear whiter than normal, which is a consequence of the increased nucleus density and size, as well as the potential change of the chromatin characters [8, 9]. The decreased stromal scattering, which is associated with a degradation of collagen fibers, also can be observed in precancerous cervical tissue [10]. At last, there's evidence that the auto-florescence spectrum in the epithelial is altered during neoplastic process [11].

Therefore, much attention is drawn to explore the feasibility of optical imaging for the detection of cervical carcinoma, by evaluating the changes in cell density, chromatin refractive index, and the level of the angiogenesis [4,6]. However, most pure optical imaging technologies either utilize the back scattered ballistic photons [12–17], or rely on the nonlinear optical phenomenon [18,19]. Due to the high scattering of the biological tissue, the penetration depth is generally limited to the most superficial epithelial layers for these methods [4]. On the other hand, cervical precancer arises originally from the bottom of cervical epithelium, and cancer cells will invade through the basement membrane and deep into the soft tissue when cancer is developed [20,21] (as shown in Fig. 1). Thus, these pure optical imaging modalities are not ideal for the early detection of CC, nor can they be used for the evaluation of the cancer invasion depth.

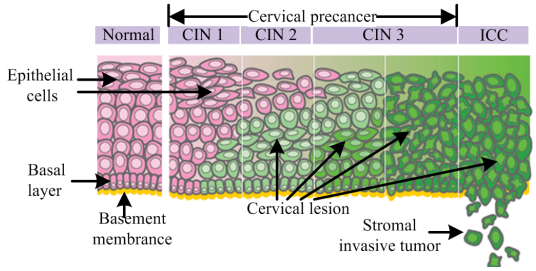

Fig. 1. Development of cervical cancer. CIN presents cervical intraepithelial neoplasia; and ICC presents invasive cervical cancer. Reprinted with permission from The National Cancer Institute of United States, D Kerrigan and colleagues [21]. Copyright 2008 NCI.

Comparatively, photoacoustic imaging (PAI) is a hybrid optical imaging modality that not only inherits the high optical contrast from pure optical imaging, but also combines the high spatial resolution and the deep imaging depth from the ultrasound imaging [22]. By utilizing the intrinsic hemoglobin as the contrast agent, it is highly sensitive to the abnormal angiogenesis which is a main character of the cancer-related change. More importantly, it employs ultrasound as the probing signal, so that it has a deeper penetration depth superior

#221095 - $15.00 USD Received 27 Aug 2014; revised 20 Oct 2014; accepted 13 Nov 2014; published 15 Dec 2014

than that of the pure optical imaging modalities. To date, PAI has been employed for the diagnosis of various cancers with different scanning configurations [23–25].

In this paper, we for the first time propose to use PAI for the diagnosis of CC. The main purpose of this paper is to test the ability of PAI to distinguish different stages of CC with intensive ex-vivo experiments, to provide solid experimental basis for the in-vivo application of cervical PAI in the future studies.

2. Materials and methods

The cervical samples in this study were provided by the gynecology department of the second Xiangya hospital (Changsha, China). A total of 30 experiments were carried out, and in each experiment one piece of normal cervical tissue and one piece of cervical lesion from the same patient were embedded in a cylindrical phantom for simultaneous PAI imaging. The samples were harvested from the cervical canal by biopsy during a cervical colposcopical screening. Immediately after the biopsy, all the samples were preserved in liquid nitrogen for later examine. Later, each frozen sample was divided into two pieces, one of which was for the PAI imaging, and the other was sent for histological evaluation for cross-validation. The staging of the lesions were determined by summarizing the results of histology, colposcopy and magnetic resonance imaging (MRI). Patients consent was obtained, and all the experimental procedures were performed in accordance with the guiding principles for research involving animals and humans of Xiangya Medical College of Center South University.

The schematic of the PAI system is shown in Fig. 2. A Q-switch Nd: YAG laser (Nimma-600, Beamtech Optronics) generated pulsed 532 nm light with a repetition rate of 10 Hz, and the pulse width was about 6 ns. The laser was delivered with a 400 μm core multimode fiber (BGWU-400, SCITLION), and then focused onto the surface of the phantom with a spot size around 1 mm in diameter. The average laser intensity of the light spot was about 17 mJ/cm^2, which is about 85% of the ANSI safety limit. The samples embedded into the phantom were about 3~6 mm in size, separated 1~2 mm from each other. The depths of the samples were about 5 mm, and this is to explore the ability of PAI for the detection of deep lesions. The phantoms were made of ager, intralipid and Indian ink [26]. The reduced scattering and absorption coefficients of the phantoms were set to be 1 $/mm$ and 0.07 $/mm$, which are similar to that of the normal cervical tissue [27]. The phantom was elevated through a 5 cm-diameter hole from the bottom of the water tank, which was covered with a 15 μm–thick polyethylene film. For the ultrasound probing, the generated ultrasound was deflected by a thin optical transparent acoustic reflector (about 1 mm) to a 10 MHz focused transducer (A312S-N-SU Olympus). The focal length of the transducer was about 10 mm, and its horizontal and axial resolutions were about 0.4 mm and 0.2 mm respectively. Then the collected photoacoustic signal was amplified by an ultrasound pulser/receiver (5072PR, Olympus), digitized with a DAQ card (LDI400SE, DIYANG, with a sampling frequency of 100 MHz), and stored on hard drive for later processing. Part of the light delivering and ultrasound collecting systems including the fiber tip, the convex lens, the transducer and the acoustic reflector were integrated into a module, and immersed in water for acoustic coupling. The module was actuated with a 2D step motor (TSA150-b, Zolix) system for x-y scanning. The step size was 0.1 mm for both x and y directions. A Labview program controlled the data acquisition process, and the whole system was synchronized by the pulsed Nd: YAG laser.

For the data processing, the data of each A-line is firstly applied with a band-pass filter of 1-7 MHz, and then truncated to extract the signal of 3~8 mm blow the phantom surface. Then the extracted signals from all the A-lines in one experiment were used to produce the depth maximum amplitude projection (DMAP) image in the x-y plane [23,24,28]. Since the thicknesses of the samples were small, and all the samples were almost located at the same depth, the DMAP images can be used to roughly represent the optical absorption distribution of the samples, to help the evaluation of angiogenesis level for the diagnosis of CC. The

#221095 - $15.00 USD Received 27 Aug 2014; revised 20 Oct 2014; accepted 13 Nov 2014; published 15 Dec 2014

margins of the samples were determined manually with the guiding of photo images taken after the PAI experiments. The mean optical absorptions (MOA) for all the samples were then calculated. Paired t-test was done to compare the MOAs between the normal tissue and tissue lesion in each stage [29]. We also studied the correlation between the MOAs and the staging of the samples with the Spearman's rank order correlation coefficient (SROCC) [30].

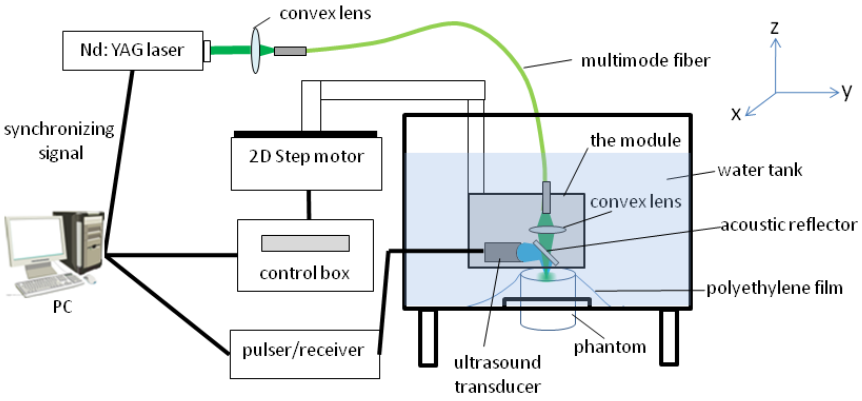

Fig. 2. Schematic of photoacoustic imaging system

3. Results

The definition of each cervical lesion stage is present in Table 1 [31], along with the experiment IDs for each stage listed. In this study, we tested 1 sample for CIN2, 6 samples for CIN3, 12 samples for CC1, 10 samples for CC2, and 1 sample for CC3. There are few samples for CIN2 and CC3, which is because it is usually not necessary to take biopsy for patient with low-grade precancer lesions, and it is also difficult to obtain healthy cervical tissue from the suspicious lesion area on patients with CC higher than stage 2.

Table 1. Cervical cancer staging definition and experimental design.

Clinical stage	Experiment ID	Classification information
CIN[a] stage 1	NaN	The lesion is confined to the basal 1/3 of the epithelium.
CIN[a] stage 2	1	The lesion is confined to the basal 2/3 of the epithelium.
CIN[a] stage 3	2~7	The lesion affects greater than the basal 2/3 of the epithelium, but is still confined to the epithelium.
CC[b] stage 1	8~19	The carcinoma is strictly confined to the cervix.
CC[b] stage 2	20~29	The carcinoma invades beyond the uterus, but not to the pelvicwall or to the lower third of the vagina.
CC[b] stage 3	30	The carcinoma extends to the pelvic wall or involves lower third of the vagina or causes hydronephrosis kidney
CC[b] stage 4	NaN	The carcinoma has extended beyond the true pelvis or has involved the mucosa of the bladder or rectum

[a]Cervical intraepithelial neoplasia; [b]Cervical carcinoma;

Representative experimental results for each stage are shown in Fig. 3. The first two rows show the histological results for the normal cervical tissue and tissue lesion respectively, and the photoacoustic DMAP images are shown in the bottom row. The corresponding photo images to the DMAP images are shown in the third row for reference, which are taken after removing the top 4 *mm* background phantom. The maximum value of the DMAP images is normalized to 1. The margins of the cervical lesion and the normal tissue are determined

#221095 - $15.00 USD Received 27 Aug 2014; revised 20 Oct 2014; accepted 13 Nov 2014; published 15 Dec 2014

manually, with the guiding of photo images that was taken after the PAI experiments, as indicated with red and green lines respectively in the both the photo and DMAP images. The scale bar for the histological images represents 0.1 *mm* , and that for the photo and DMAP images is 1 *mm* .

Nuclear enlargement with variation in size and shape is a regular feature of all dysplastic cells. Increased intensity of staining (hyperchromasia) is another prominent feature; irregular chromatin distribution with clumping is always present in dysplastic cells; the proportion and distribution of the dysplastic cells are increasing as the lesion develops towards cancer [32]. Correspondingly, it's noticed that the signal intensity of the cervical lesion is significantly higher than that of the normal tissue in the DMAP images.

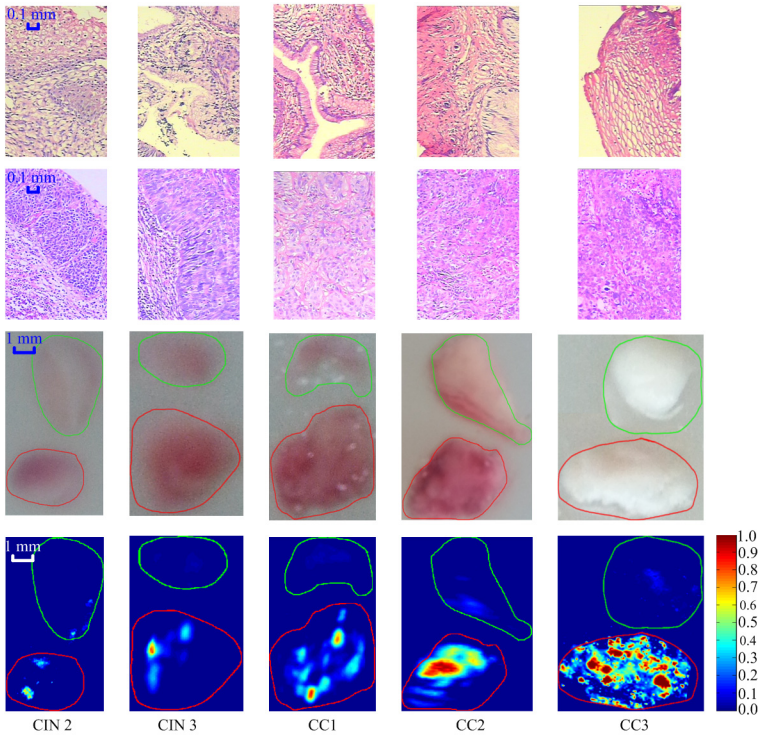

Fig. 3. Comparison between the normal cervical tissue and tissue lesion for different stages. From top to bottom are the pathological images for the normal cervical tissue (first row) and tissue lesion (second row), the photo image (third row) and corresponding DMAP images (fourth row) of representative experiments respectively. Margins of the normal tissue (green) and cervical lesion (red) are indicated in the photo and DAMP images. The scale bar for the histological images represents 0.1 *mm* , and that for the photo and DMAP images is 1 *mm* .

#221095 - $15.00 USD Received 27 Aug 2014; revised 20 Oct 2014; accepted 13 Nov 2014; published 15 Dec 2014

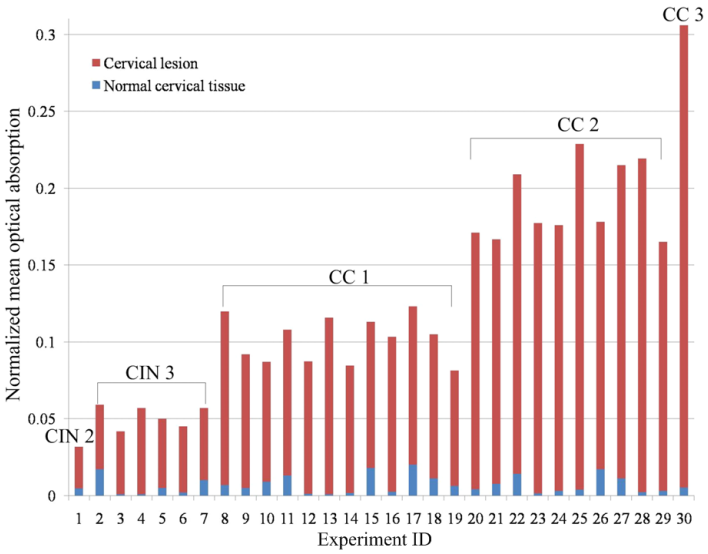

Fig. 4. Normalized mean optical absorption for all the samples.

For statistical analysis, mean signal intensities for all the samples were calculated which were taken as the MOAs, as shown in Fig. 4. Then paired t-test were calculated for each stage and across all the stages to assess the difference of the MOAs between the normal tissue and tissue lesion, as listed in Table 2. Results show that the MOA of the tissue lesion is significantly higher than that of normal tissue for all the stages in our study (with a confidential coefficient P = 0.05). This could be explained by the fact that the angiogenesis level and hemoglobin concentration are higher in cervical lesion than the normal tissue to support the growth of dysplastic cells.

Table 2. Statistical results for different stages of cervical lesion

Stage of the sample	t value of MOA[c]
CIN[a] stage 2	NaN
CIN[a] stage 3	$\|11.47\| > t(10, 0.05) = 2.$
CC[b] stage 1	$\|20.79\| > t(22, 0.05) = 2$
CC[b] stage 2	$\|22.32\| > t(18, 0.05) = 2$
CC[b] stage 3	NaN
Total	$\|9.09\| > t(58, 0.05) = 2.($

[a]Cervical intraepithelial neoplasia; [b]Cervical carcinoma; [c]Mean optical absorption; The t-values were calculated with the paired t-test for comparison in the mean optical absorption between the cervical lesion and the normal tissue (confidential coefficient P = 0.05).

In Fig. 4, it's also noticed that the MOAs increase almost monotonically with the severity of the lesions. We investigated the correlation relationship between the staging and the MOA of the samples with the SROCC across all the stages, which was calculated to be as high as 0.9431 in our study.

4. Discussion and conclusion

In current clinical practice, the cervical lesion detection is mainly through cervical screening, along with the following biopsy. Although with the colposcopy, this method can efficiently detect cervical lesions originally from the superfical regions around the external orifice, there

#221095 - $15.00 USD Received 27 Aug 2014; revised 20 Oct 2014; accepted 13 Nov 2014; published 15 Dec 2014

is few means for the detection of cervical lesions in the cervical canal. Cervical canal is about 50 *mm* long with an internal diameter of 2~3 *mm*, so that the direct observation of cervical canal is almost impossible under the colposcopy [5]. Besides, the assessment of invasion depth of cancer cells is of critical importance to the treatment strategies [32]. Cancer cells can invade much deep into the soft tissue, which can be true for cervical lesions both around the external orifice and in the cervical canal [5]. However, cervical screening can only see superficial lesions [5]. Therefore, there's a strong demand to develop new technologies for the diagnosis of CC.

Compared with the cervical screening based methods, PAI has a much higher penetration depth by utilizing less scattered ultrasound as the probing signal, so that the optical absorption distribution that is directly proportional to the angiogenesis level can be obtained deep in the biological tissue. In our experiments, the MOAs of normal tissues are quite small (all<0.025), and lesions of higher than CIN 2 can be well distinguished even at a depth of 5 *mm*. Results also show that there's strong correlation between the MOA and the staging of the lesions. All these results indicate that with fixed light intensity and depth, PAI is potential for the detection of cervical lesions, as well as the staging evaluation, by judging the MOAs of the lesions. With high repetition lasers and appropriate scanning schemes, intact fast scanning over the whole cervix can be realized with PAI for the diagnosis of CC.

Although our ex-vivo results are encouraging, the feasibility of PAI in the diagnosis of CC still needs to be proved with in-vivo experiments. Our main interest is to adapt the PAI system for the endoscopic scanning in the cervical canal. The endoscopic photoacoustics has always been a main branch in the field of photoacoustic research, which has already been demonstrated in the imaging of vascular and esophagus [33,34]. Small endoscopic photoacoustic catheter with a diameter of 2.5 *mm* has been reported [34]. Because the majority of the patients with CC are women who have had babies, their cervical canals can be expanded easily. In our applications, a probe smaller than 10 *mm* in diameter would be thought to meet the needs, so it's viable in technique for the endoscopic photoacoustic imaging of the cervix. Acoustic coupling can be ensure with the tight contact of the cervical tissue to the photoacoustic catheter due to the cervical canal contraction, and disposable sleeves for the catheter can be employed for hygiene considerations. The study of the cervical endoscopic probe has already been carried out in our lab. It's noted that although our intention is to do the diagnosis of CC solely with PAI, because this method has not been tested in in-vivo experiments, we would likely to use it for the guiding of biopsy as an initial step. Following studies of this work will be reported later.

There are limitations in this work. The case number in our ex-vivo study is still limited, especially for CIN2 and CC3. Besides, our data analysis is based on the DMAP images, which is only an approximation to the exact absorption distribution when the sample size is small in the z direction. This might be improved if we could calculate the absorption coefficient in the three dimensional space using more complicated algorithms such as the finite element based quantitative photoacoustic algorithm coupled with the photon diffusion equation [35].

In summary, we for the first time propose to employ PAI for the diagnosis of CC, and preliminarily explored its potential with extensive in-vitro experiments. Results shows that the cervical lesions can be well distinguished at the depth of 5mm even for CIN2, and the signal intensity of PAI increased significantly with the development of CC, which mean that PAI may promise for the diagnosis of CC.

Appendix

Paired t-test

In this study, paired t-test was done to study the difference in the mean MOAs between the normal cervical tissue and tissue lesion for different stages. Given that the MOAs of the

#221095 - $15.00 USD Received 27 Aug 2014; revised 20 Oct 2014; accepted 13 Nov 2014; published 15 Dec 2014

normal cervical tissue and tissue lesion are represented with data groups x_1 and x_2 respectively, the t values are calculated as follows:

$$t = \frac{\overline{x}_1 - \overline{x}_2}{\sqrt{\left(s_{x_1}^2 + s_{x_2}^2\right)/n}} \tag{a.1}$$

Here $\overline{x}_1$ and $\overline{x}_2$ are the mean values of x_1 and x_2 respectively, and s_{x_1} and s_{x_2} are the unbiased estimators of the variances of the two data groups. n is the experiment number for each stage. For significance testing, the freedom of this test is $2n-2$.

The Spearman's rank order correlation coefficient

The SROCC was used to study the correlation between the MOAs of the tissue lesions and their staging levels across all the lesion stages.

Firstly, we valued the staging of CC from CIN 2 to CC 3 to be 1 to 5 according to the lesion severity, and then two $N\times 1$ vectors are introduced:

$$\begin{aligned} \mathbf{x} &= \{x(1), x(2), \cdots, x(N)\}^{\mathrm{T}} \\ \mathbf{y} &= \{y(1), y(2), \cdots, y(N)\}^{\mathrm{T}} \end{aligned} \tag{a.2}$$

Here $x(i)$ and $y(i)$ represents the MOA and the staging of the tissue lesion respectively, with i to be the experiment ID, and the total number of experiments N is 30.

Next, the rank-order vectors $\mathbf{r_x}$ and $\mathbf{r_y}$ are generated for the two vectors respectively. The value for the vector unit $r_x(i)$ can be calculated as follows:

$$r_x(i) = 1 + a_i + \frac{1}{b_i}\sum_{k=0}^{b_i-1} k \qquad i = 1, 2, ..., N \tag{a.3}$$

Here a_i is the number of data in $\mathbf{x}$ that are larger than $x(i)$, and b_i is the number of data in the vector $\mathbf{x}$ that are equal to $x(i)$. Similarly, the vector units of $\mathbf{r_y}$ can also be calculated.

Finally, the SROCC between the MOA and staging of the tissue lesions can be obtained by calculating the cross-correlation coefficient between vector $\mathbf{r_x}$ and $\mathbf{r_y}$, as:

$$\mathrm{SROCC} = \frac{\sum_{i=1}^{N}(r_x(i)-\overline{r}_x)(r_y(i)-\overline{r}_y)}{\sqrt{\sum_{i=1}^{N}(r_x(i)-\overline{r}_x)^2}\sqrt{\sum_{i=1}^{N}(r_y(i)-\overline{r}_y)^2}} \tag{a.4}$$

Where $\overline{r}_x$ and $\overline{r}_y$ are the mean of vector $\mathbf{r_x}$ and $\mathbf{r_y}$, respectively.

Acknowledgments

This study was funded by the National Natural Science Foundation of China (Grant No. 31200748); the National Natural Science Foundation of China (Grant No. 61401520); the Postdoctoral Science Fund of Central South University (Grant No. 20120312).